Encompassing Filtering Effects in Transceiver Models for Converged Metro-Access Networks

Encompassing Filtering Effects in Transceiver Models for Converged Metro-Access Networks

1st Andrea Rosso
DET, Politecnico di Torino
Turin, Italy
andrea.rosso@polito.it

2nd Enrico Miotto
DET, Politecnico di Torino
Turin, Italy
enrico.miotto@polito.it

3rd Emanuele Virgillito
DET, Politecnico di Torino
Turin, Italy

4th Stefano Straullu
LINKS Foundation
Turin, Italy

5th Francesco Aquilino
LINKS Foundation
Turin, Italy

6th Andrea Castoldi
SM-Optics
Cologno Monzese, Italy

7th Raffaele Corsini
SM-Optics
Cologno Monzese, Italy

8th Vittorio Curri
DET, Politecnico di Torino
Turin, Italy

***Abstract*—We present a comprehensive experimental analysis of filtering penalties in metro-access scenarios, characterized by cascades of ROADMs and optical amplifiers. This analysis evaluates the impact of various configurations, considering filter bandwidths, data rates, and received optical power.**
The novelty of this work lies in the derivation and validation of a transceiver model that encompasses filtering penalties, along with the application of this model to facilitate end-to-end lightpath deployment in converged network-as-a-service environments for fog computing, aiming to enhance spectral efficiency.

***Index Terms*—Filtering penalty, transceiver modeling, equalization, metro access networks, edge datacenters**

I. Introduction

Cloud computing has transformed data and service delivery by offering scalable, on-demand resources through centralized data centers. However, the rising demand for low-latency applications like IoT, edge computing, and real-time analytics has exposed the limitations of traditional cloud models, particularly in managing large data volumes at the network edge. This has led to the rise of fog computing [1], a paradigm that decentralizes processing and storage to edge data centers (EDC) [2], requiring high-capacity, low-latency end-to-end (E2E) data channels.

The continuous growth of fiber optic infrastructure in metro and access networks, traditionally separate, offers a seamless opportunity for such data connection requests if infrastructure convergence is enabled by removing opaque nodes, as shown in [3], and through orchestrated optical control architectures, thus enabling the network-as-a-service (NaaS) paradigm [4]. To achieve this, an accurate quality-of-transmission digital twin (QoT-DT) of the converged networks is essential to ensure precise performance metrics for any cross-segment E2E lightpath, such as the generalized SNR (GSNR), the received optical power (ROP), latency, and GSNR penalties.

In metro scenarios, traversing multiple reconfigurable optical add-drop multiplexer (ROADM) nodes may introduce non-negligible filtering penalties, which have been shown to depend on the filtering sites, the positions of noise sources and the coherent digital signal processing (DSP)-based receiver performance [5], [6]. Moreover, in addition to the need for an accurate QoT-DT, a precise model for the transceiver (TRX) is essential. In [7], an analytical model of BER versus both the GSNR and intrinsic transceiver *SNR* —dependent on the received optical power (ROP)— is presented and experimentally validated, while the effects of filtering penalties, crucial for the scenario at hand, have not yet been fully clarified and integrated with a general transceiver model.

In this work, we aim to fill this gap. First, we perform experimental characterizations on the effects of cascaded commercial ROADM's optical filters at different sites introducing noise. Based on this characterization, we clarify how to precisely include the filtering effect in the TRX model. Then, we consider a possible E2E connection traversing a metro segment and relying on a passive link to reach an EDC.

We demonstrate how the high spectral efficiency enabled by the WDM flex-grid down to 37.5 GHz can impact the maximum passive link length. Thus, the metro-access NaaS offers a solid opportunity that requires a common QoT-DT relying on open interfaces, as well as accurate TRX modeling that encompasses all impairments. This approach can enable an innovative operational methodology to evaluate the feasibility of deploying lightpaths in cross-segment converged networks.

II. Experimental modeling of transceiver and filtering effect characterization

For the experimental study, we used a pluggable transceiver capable of generating 100, 200 and 400 Gbps signals based on DP-QPSK and DP-16QAM modulations in a white-box transponder. The performances of the transceiver are fully characterized by the bit error rate (BER) in the equation:

$$\mathrm{BER} = a_1 \,\mathrm{erfc}\sqrt{a_2\, SNR} \tag{1}$$

where a_1 and a_2 coefficients depend on the selected modulation format. [8] *SNR* represents the overall signal to noise ratio on the electrical signal after the DSP receiver, straight before the forward error correction (FEC) stage: in general, its reciprocal is obtained as the summation of the reciprocals of SNR_{TX} and SNR_{RX} due to the transceiver implementation, the SNR_{ASE} from noise injected by the amplifiers and SNR_{NLI} from fiber propagation. In this work we assume the absence

978-3-903176-67-6 © 2025 IFIP

of Non Linear Interference (NLI), which is common in metro and access networks characterized by short links and low optical power level, and therefore, we neglect the SNR_{NLI} term in the *SNR* expression. In this study, all the *SNRs* noise bandwidths are computed on the symbol rate R_s to make the chosen modulation configurations comparable. In this sense $SNR_{\text{ASE}} = OSNR \cdot \frac{B_n}{R_s}$, where *OSNR* is the ASE noise contribution calculated in the traditional noise bandwidth B_n = 12.5 GHz. In addition, the overall effect of SNR_{TX} and SNR_{RX}, defined as SNR_{TRX}, can be characterized by a preliminary back-to-back (B2B) data collection (Fig. 1b). In particular, only its SNR_{RX} component is function of ROP, and it is considered predominant with respect to SNR_{TX}: as a consequence, in the following sections, SNR_{TRX} contains both the contributions and it is located in the receiver's position. In order to perform its characterization, the transceiver under test is connected in a loop such that the transmitted signal traverses a variable optical attenuator (VOA) before reaching the receiver. This configuration enables the systematic evaluation of multiple ROPs through controlled adjustments to the VOA's configuration, obtaining the correspondence between a large set of ROP values and the BER measured from the transceiver. Then, since SNR_{TRX} is considered the only contribution in the B2B setup, it is possible to invert Eq. 1 obtaining a relation between the ROP and the SNR_{TRX} itself. Finally, the obtained curves can be fitted over an analytical function describing the coherent optical transceivers as in [7] obtaining a complete model of the specific transceiver under test, as represented in Figure 1b.

A. Experimental setup

The experimental setup used to study the filtering effects is presented in Fig. 1a: the signal propagates through three commercial ROADM's optical filters, whose channels are centered at the same nominal frequency as the channel under test (CUT), determining a dual-sided symmetric filtering condition. The filter widths are reconfigurable in steps of 12.5 GHz, starting from a minimum of 37.5 GHz, and their constant attenuation is fully compensated by a booster amplifier (BST) located in the beginning of the line. The transmitted power from the transceiver has been set to 0 dBm. In order to evaluate the trade-off between spectral efficiency and filtering penalty, we focused on DP-16QAM at 200 and 400 Gbps, generated and received using commercial transceivers. We compare the 37.5, 50 and 75 GHz filters on the 31.6 and 63.1 Gbaud signals, which are characterized by a roughly equal spectral efficiency. Furthermore, the system allows for independent control of four noise sources using VOA at each amplifier stage. They have been calibrated such that the SNR_{ASE} is equal between the four noise sources when measured at the receiver. The BER has been measured for different values of ROP (between -15 dBm and -25 dBm). For each ROP value, the BER has been measured varying the SNR_{ASE} using the VOAs. Additionally, an optical spectrum analyzer (OSA) is employed to capture the signal spectrum and measure its *OSNR*.

From the modeling point of view, the *SNR* is fully defined by Eq. 2, in which an additional set of coefficients k_i are introduced to account for the filtering effects [5].

$$\frac{1}{SNR} = \frac{k_{\text{TX}}}{SNR_{\text{TX}}} + \frac{k_{n_1}}{SNR_{\text{ASE,1}}} + \frac{k_{n_2}}{SNR_{\text{ASE,2}}} + \\ + \frac{k_{n_3}}{SNR_{\text{ASE,3}}} + \frac{k_{n_4}}{SNR_{\text{ASE,4}}} + \frac{k_{\text{RX}}}{SNR_{\text{RX}}} \quad (2)$$

Whenever a signal is filtered, its shape is modified according to the filter's transfer function, and then the receiver's equalizer attempts to restore its original shape by performing equalization based on a new transfer function whose actual shape depends on the receiver strategy [9]. As the synthesized equalizer response recovers the entire filters cascade, ASE noise contributions that have not traversed the entire filter cascade are amplified after receiver equalization.

This affects the received signal quality: consequently, the most severe penalties are introduced when more ASE noise is injected closer to the receiver, as these noises are filtered less than the signal. Therefore, they are characterized by a larger k_i. On the contrary, noise contributions added before the filter cascade subdue the same overall filtering effect and they are completely restored at the receiver, so they do not get enhanced. This leads to having $k_{\text{TX}} = k_{n_1} = 1$ and $k_{n_4} = k_{\text{RX}}$.

B. Optical filters modeling from experimental data

Before computing analytically the coefficients k_i of Equation 2, which is the target of Section II-C, the spectrum response of optical filters has been modeled according to [10], which is an improvement compared to the general simplified Super-Gaussian model for ROADM's optical filters adopted in [5]. The filter field spectrum is expressed by:

$$S(f) = \frac{1}{2}\sigma\sqrt{2\pi}\left[\text{erf}\left(\frac{\frac{B_{\text{ch}}}{2} - f}{\sigma\sqrt{2}}\right) - \text{erf}\left(\frac{-\frac{B_{\text{ch}}}{2} - f}{\sigma\sqrt{2}}\right)\right] \quad (3)$$

Where B_{ch} is the channel bandwidth and $\sigma = \frac{BW_{\text{OTF}}}{2\sqrt{2ln2}}$. As suggested in [10], the OSA traces of filter spectra have been fitted tuning the BW_{OTF} parameter, leading to the filter transfer functions depicted in Figure 1c. All the three filters included in the experimental setup cascade are identical, therefore just the spectra of one of them is reported. The filter spectra are computed from the input and output signal spectra, measured with the OSA, for different filter bandwidths in absence of ASE noise. Some misalignment occurred between the input and output signal spectrum measurements, due to a slight frequency jitter of the transceiver between the two measurement instants, causing the small peaks in the filter spectra flat region. The chosen approach has been to fit in a conservative way, thus, the modeled spectra are slightly narrower at the border of the experimental data. The adopted values of BW_{OTF} are provided in Figure 1c.

C. Filtering penalty coefficients computation

The starting point for the analytical determination of the coefficients in Equation 2 is the block diagram shown in Figure 2a. The experimental setup depicted in Figure 1a has been theoretically replicated, incorporating some simplifying assumptions, in addition to the absence of NLI previously anticipated. Attenuation has been neglected, since it operates

equally on signal and noise, without affecting the *SNR* or the filtering penalty.

First, it is assumed that transmitter impairments are generally much smaller than receiver impairments, according to what stated before. Consequently, all the filtering penalty affecting the transceiver *SNR* are considered at the receiver side, represented by an appropriate k_{TRX}, which must be computed. Furthermore, the optical front end (OFE), based on coherent receiver principle, is assumed to convert the optical signal into electrical without additional filtering impairments. This implies that both the ASE introduced at the receiver side (source number 4 in Figure 2a) and the noise introduced by the transceiver (which is mainly due to OFE's photodiodes noise) are not filtered, so they incur in the same penalty when equalizer applies its effect on them. As a result, $k_{n_4} = k_{\text{TRX}}$. As a consequence, Equation 2 reduces to Equation 4, where $k_1 = k_{n_1}$, $k_2 = k_{n_2}$, $k_3 = k_{n_3}$, $k_4 = k_{n_4} = k_{\text{TRX}}$:

$$\begin{aligned} \frac{1}{SNR} &= \frac{k_{\text{ASE}}}{SNR_{\text{ASE}}} + \frac{k_{\text{TRX}}}{SNR_{\text{TRX}}} = \\ &= \frac{k_1}{SNR_{\text{ASE},1}} + \frac{k_2}{SNR_{\text{ASE},2}} + \\ &\quad + \frac{k_3}{SNR_{\text{ASE},3}} + \frac{k_4}{SNR_{\text{ASE},4}} + \frac{k_4}{SNR_{\text{TRX}}} \end{aligned} \tag{4}$$

The second assumption is that all noise sources are characterized by a flat power spectral density (PSD) with a value of $\sigma^2_{ASE_i}$ (where $i = 1, 2, 3, 4$) for ASE sources and σ^2_{TRX} for the transceiver, at least within the signal bandwidth. In our case, with equally-distributed noise among the ASE sources, it is possible to compute the PSDs based on the desired SNR_{ASE} and the characterized SNR_{TRX} in the signal symbol rate, exploiting the fact that we neglect attenuations so that the power remains constant along the line:

$$\sigma_i^2 = \frac{P_{\text{TX}}}{4 \cdot SNR_{\text{ASE}} \cdot R_s} \qquad \sigma^2_{\text{TRX}} = \frac{P_{\text{TX}}}{SNR_{\text{TRX}} \cdot R_s} \tag{5}$$

Where we set $P_{\text{TX}} = 0$ dBm equal to the one of the transceiver in the experiment and R_s is the signal symbol rate (equal to 31.6 Gbaud or 63.1 Gbaud). The factor 4 at the denominator of σ_i^2 expression accounts that noise is equally distributed among the ASE sources.

The third assumption is about the models chosen for each filtering device. The filtering effect experienced by the signal and noise in each ROADM is modeled as in Section II-B. The shaping filter, on the other hand, is modeled as a square root raised cosine.

The final assumption concerns the DSP at receiver side, which is assumed to perform both matched filtering and equalization, operating at a sampling rate equal to 2 Samples per Symbol (SpS), so that no overlapping is present on the spectrum of sampled signals crossing the equalizer. The output equalizer signal is then sampled again at 1 SpS to recover the original symbol sequence. For simplicity, we assume the Zero Forcing Equalizer (ZFE) with infinite number of taps as the equalizer strategy [9]. We underline that the peculiar equalizer strategy and the number of taps implemented in the real transceiver DSP can be in general unknown due to closed source nature of DSP implementation. We choose here the ZFE instead of a more realistic minimum mean square error (MMSE) equalizer strategy as it is easier to model and provides theoretically worst case filtering penalties.

The initial step of the analysis involves evaluating the evolution of noise along the link. Even though the noise sources are white, the filtering effect applies both on signal and noise. The overall result is that the data signal becomes distorted, and the noise is no longer white. Specifically, at the receiver side, the perceived noise is the sum of multiple "colored" components due to the additive nature of noise. Each of these components is colored based on the number and shape of filters it has passed through. Using the well-known formula for computing the PSD of processes crossing filters, it is possible to derive the receiver-side equivalent noise normalized PSD before sampling:

$$PSD_{\text{ASE+TRX}}(f) = \frac{\sum_{i=1}^{N_{\text{filt}}+1} \sigma_i^2 \cdot \prod_{n=i}^{N_{\text{filt}}} |H_n(f)|^2}{\sigma^2_{\text{ASE+TRX}}} \tag{6}$$

where $\sigma_i^2 = \sigma^2_{\text{ASE}i}$ for $i = 1, 2, 3$ and $\sigma_4^2 = \sigma^2_{ASE_4} + \sigma^2_{\text{TRX}}$, and $N_{\text{filt}} = 3$. The total noise PSD in Equation 6 has been normalized by the factor in Equation 7:

$$\sigma^2_{\text{ASE+TRX}} = \sum_{i=1}^{N_{\text{filt}}+1} \sigma_i^2 \tag{7}$$

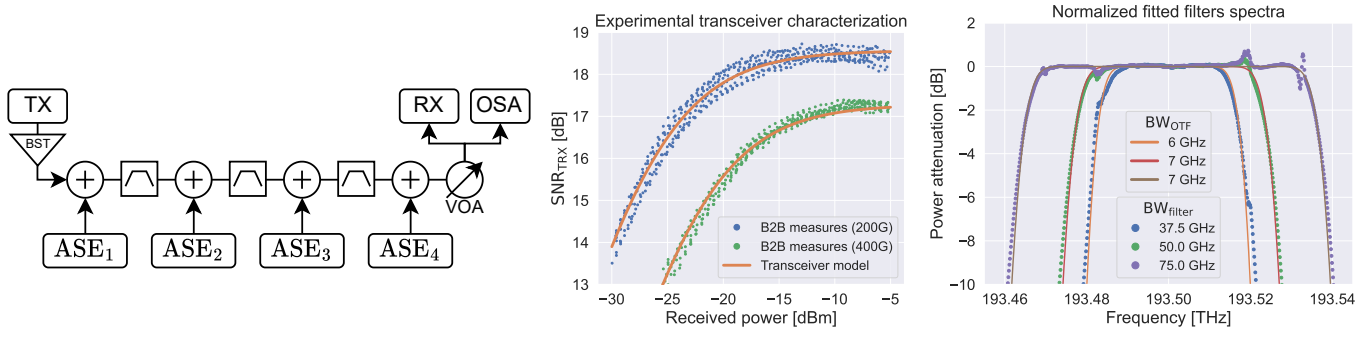

(a) (b) (c)

Fig. 1: (a) Experimental setup. (b) Transceiver characterization. (c) Filters spectra and corresponding fitted model.

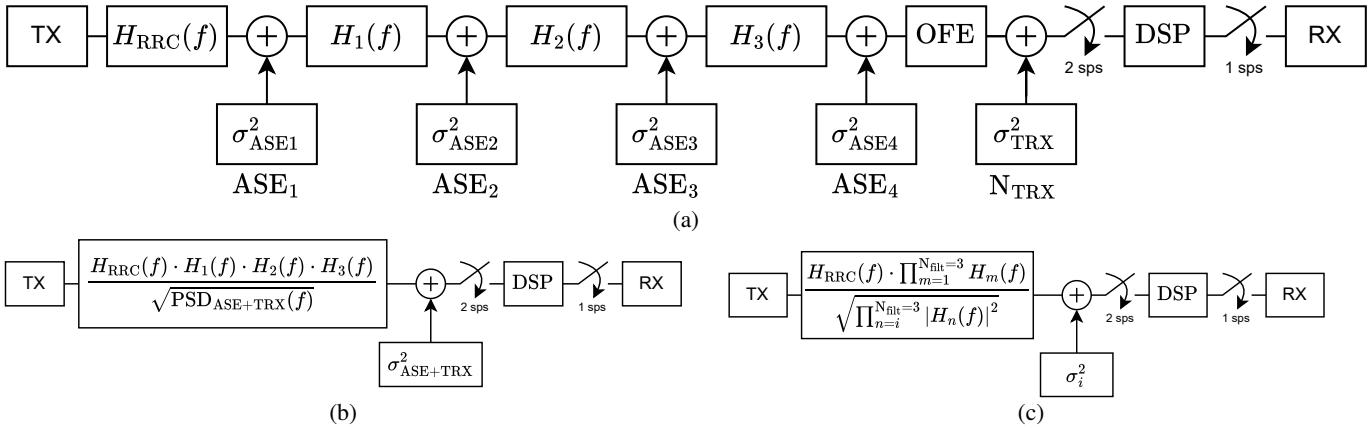

Fig. 2: (a) Block diagram of the reference theoretical model. (b) White noise equivalent model. (c) Disaggregated model.

This operation is necessary in order to simplify the model by considering its white noise equivalent block diagram, which is provided in Figure 2b. The idea is very common in equalization theory [9]: the colored noise can be whitened if the colored noise PSD has an invertible square root, which is valid in the current case where it is composed by products of linear filters and scaling factors. Thanks to the normalization factor, the equivalent white noise source at receiver side PSD is $\sigma^2_{\mathrm{ASE+TRX}}$. Once the white noise equivalent model is built, it is possible to select the DSP transfer function (in D-domain [9]) in order to perform matched filtering and zero forcing equalization:

$$W_{\mathrm{DSP}}(D) = \frac{H_{\mathrm{RRC}}(D)\cdot\sqrt{PSD_{\mathrm{ASE+TRX}}(D)}}{H_1(D)\cdot H_2(D)\cdot H_3(D)} \tag{8}$$

Now that all the key assumptions on the system and on the devices have been set, the *SNR* after equalization can be computed according to the following formula:

$$SNR = \frac{SNR_{\mathrm{ASE+TRX}}}{k_{\mathrm{TOT}}} \tag{9}$$

Where $SNR_{\mathrm{ASE+TRX}}$ is obtained by Equation 4 with $k_i = 1$ (e. g. no filtering, just ASE injection and transceiver penalty), therefore it is known. The total impairment due to filtering in the case of ZFE can be computed as:

$$k_{\mathrm{TOT}} = \frac{1}{R_s}\int_{-R_s}^{R_s}\left|W_{\mathrm{DSP}}\left(e^{j\frac{\pi f}{R_s}}\right)\right|^2 df \tag{10}$$

Equations 9 and 10 follow by the computation of the noise variance after sampling and DSP processing, in order to derive the filtering-affected *SNR* after equalization [9]. The final step of the analysis is the disaggregation of k_{TOT} into the sequence of k_i of Equation 4. The considered white noise equivalent system is characterized by additive Gaussian noise and linear filtering. Therefore, the disaggregation can be performed by considering each noise source characterized by σ_i^2 $(i = 1, 2, 3, 4)$ individually, and computing the corresponding constant k_i through Equation 10, with the other sources injecting no noise. This procedure leads to the disaggregated model shown in Figure 2c. It is important to note that, in this case, the disaggregated colored PSD to be considered in the channel block is solely the contribution corresponding to σ_i^2 in the general PSD equation 6. The final formula for computing k_i is then:

$$k_i = \frac{1}{R_s}\int_{-R_s}^{R_s}\frac{\left|H_{\mathrm{RRC}}\left(e^{j\frac{\pi f}{R_s}}\right)\right|^2\prod_{n=i}^{N_{\mathrm{filt}}}\left|H_n\left(e^{j\frac{\pi f}{R_s}}\right)\right|^2}{\prod_{m=1}^{N_{\mathrm{filt}}}\left|H_m\left(e^{j\frac{\pi f}{R_s}}\right)\right|^2}df \tag{11}$$

D. Experimental data and analytical model comparison

Figure 3 illustrates the comparison between the analytical model derived in Section II-C and experimental data points. As anticipated, different filter bandwidths (37.5 GHz, 50 GHz and 75 GHz), symbol rates (31.6 GHz and 63.1 GHz) and ROP (-15 dBm, -22.5 dBm and -25 dBm) have been considered. Regarding the measurements with R_s = 63.1 GHz, only the data for a filter bandwidth of 75 GHz are available, since narrower filters prevented the card operation because the filtering penalty was too strong with DP-16-QAM.

The plots are displayed with respect to the well-known Q factor [11], which is computed from the measured BER points according to Equations 12 and 13:

$$Q = \sqrt{2}\cdot erfcinv(2\cdot \mathrm{BER}) \tag{12}$$

$$Q^2_{dB} = 10\cdot\log_{10}(Q^2) \tag{13}$$

Regarding the analytical model, after computing the *SNR* through Equations 11 and 4, BER values are obtained with the well-known theoretical formula: [12]

$$\mathrm{BER} = \frac{3}{8}\mathrm{erfc}\sqrt{\frac{1}{10}SNR} \tag{14}$$

Considering the DP-16QAM modulation, where *SNR* is computed in the filter configurations under exam. Then Equations 12 and 13 are applied to the BER values in order to compute the corresponding Q^2_{dB}. Additionally, the theoretical curves in absence of filters (in dashed line in Fig. 3) are presented as a reference corresponding to the condition of no filtering penalty. Such curves derive directly from the the transceiver characterization in Figure 1b which allows the determination of SNR_{TRX} for any ROP. Subsequently, the BER (and consequently the Q) can be computed using Eq. 14 considering $SNR^{-1} = SNR^{-1}_{\mathrm{ASE}} + SNR^{-1}_{\mathrm{TRX}}$.

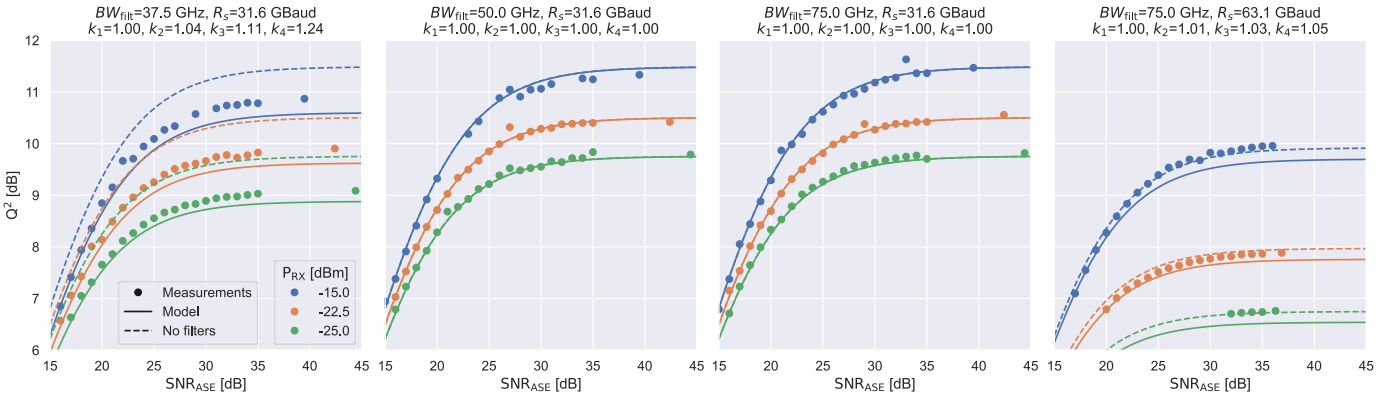

(a) (b) (c) (d)

Fig. 3: Experimental measurements and analytical model comparison with different filter bandwidths, symbol rates and ROP.

Overall, the analytical model accurately fits the experimental data with a conservative margin when the filtering effect is more intense. The first consideration, confirming the model goodness, is that model curve and experimental points are superposed when filters bandwidths are considerably larger than the symbol rate, in accordance to the theoretical curve in absence of filters. The conservative margin that can be noticed in Figures 3a and 3d between the model curves and the experimental data is due to the conservative modeling of filters performed in Section II-B. Moreover, the differences between experimental data and the derived model are also due to the chosen infinite-length ZFE equalizer, which is different from the real transceiver condition.

Focusing on Figures 3a to 3c, it can be observed that, as filtering effect intensifies, the quality factor Q decreases and the k_i values increase and differ from 1, with $k_i < k_{i+1}$ as expected. Furthermore, for each filter bandwidth, the same values of k_i have been obtained for all the considered ROP values, and thus can be considered independent on ROP. This indicates that in the considered cases, the sole cause of Q decrement depends on the receiver sensitivity, which is fully accounted for in the SNR_{TRX} characterization, calculated as a function of ROP.

Additionally, the curves in Figure 3d exhibit a worse Q factor because the larger bitrate configuration is characterized by a stronger transceiver penalty, which is modeled as a smaller SNR_{TRX} in Figure 1b.

III. Application to Convergent and Metro-Access Networks Use Case

This section examines a practical application involving an edge data center (EDC) connected to a metro network via a passive optical link. This configuration enables low-latency data access in conjunction with a larger, off-site data center (DC), a setup that is becoming increasingly relevant in the development of Fog Computing [1], [2]. An example is shown in Fig. 5a: the main DC is connected with an active link to the metro network, in which the signal transparently crosses three ROADMs and finally follows a passive link to reach the EDC. This configuration resembles the experimental setup in Fig. 1a, where the optical filters represent the overall ROADM's transfer function and the VOA simulates the attenuation of the passive link. Additionally, the ASE sources account for the noise introduced by the active link and the one of the pre- and booster amplifiers typically present in any ROADM configuration. One of the characteristics of the metro network is to maximize spectrum utilization by packing a considerable number of channels side by side. In this condition, the optical routing is performed by the ROADMs by employing tight filters around the channels of interest, resulting in strong filtering penalty effects.

Fig. 4a illustrates the practical filtering effect on a 31.6 GHz signal when the nominal filter width is set to 37.5 GHz. In particular, it demonstrates that the filter's shape causes spectral narrowing at the edges even when the filter is larger than the input signal itself, and a more pronounced effect is observable when multiple filters are applied sequentially. A similar observation can be made with a 400G signal and 75 GHz filters (Fig. 4b): when both signal and filter bandwidths are doubled, the filtering behavior around the edges remains consistent but affects a broader frequency range.

Under these conditions, an important objective is to determine the maximum distance from the metro network at which an EDC can be positioned while ensuring the minimum required performance. In practice, the most notable limitation is due to the received power: in fact, when the distance

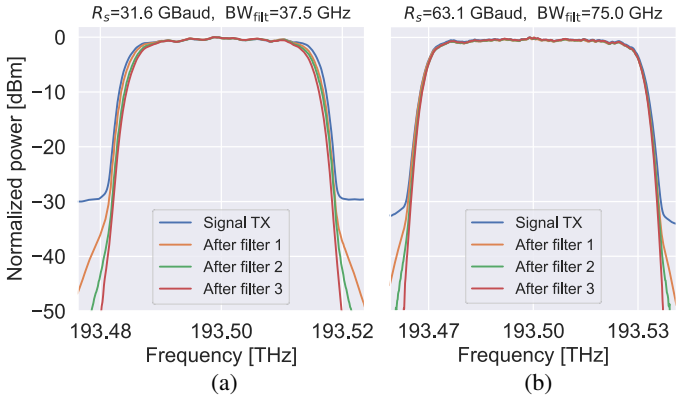

(a) (b)

Fig. 4: OSA spectrum of the transmitted and filtered signal for both the considered symbol rates.

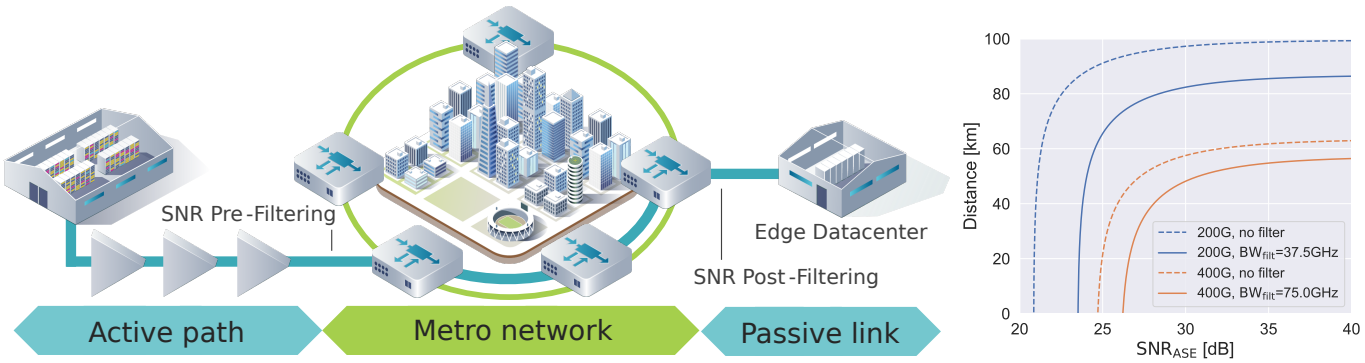

(a) (b)

Fig. 5: (a) Pictorial representation of a metro network configuration; (b) Achievable distance variation with filtering effects.

increases, the additional power loss causes a reduction in the ROP that reduces the transceiver's ability to correctly decode the signal. Although this effect is modeled as in Fig. 1b, if all the other terms in the line remain constant, a reduction of the ROP causes in turn an increase in the BER, which is always upper-bounded by the FEC algorithm implementation: this, in fact, determines the maximum achievable distance with the setup under test. In this section it is provided a practical example in which the target BER is set to 10^{-3}, the power after the last ROADM of the line is 0 dBm, and the fiber attenuation is 0.25 dB/km. For every value of the SNR_{ASE} of the line, the minimum SNR_{TRX} can be computed by inverting Equation 4 in the specific condition under test, and then the transceiver's model can be used to obtain the corresponding ROP. Finally, the maximum distance L can be easily obtained by inverting:

$$P_{\text{RX}}^{\text{dBm}} = P_{\text{TX}}^{\text{dBm}} - \alpha^{\text{dB/km}} \cdot L^{\text{km}} \tag{15}$$

The resulting relationship is shown in Figure 5b, where it is evident that for each combination of signal spectrum and filter width, there is a defined relationship between the SNR_{ASE} of the line and the maximum allowable distance.

Additionally, apart from the SNR_{TRX}, the coefficients k_i that characterize the filtering effect are crucial in determining the achievable distance. Specifically, a narrower filter leads to a significant reduction in the maximum distance, particularly at lower SNR_{ASE} values.

It is also noteworthy that the configurations compared in Figure 5b are characterized by a double symbol rate and double filter width. For this reason, this allows for the establishment of two parallel 200G links, with their corresponding filters, in lieu of the 400G link, maintaining an overall equal spectrum occupation and data rate. This enables the utilization of considerably longer passive links and accommodates the deployment of two non-contiguous frequency channels. Conversely, the single wider channel configuration necessitates the use of a single transceiver, with the reduced flexibility being offset by a reduction in cost and power consumption.

IV. Conclusion and Further Improvements

This study aims to emphasize the significance of the filtering penalty in DWDM and metro network applications, where the increasing demand for channel density necessitates the use of narrow optical filters around data channels. We derived a rigorous analytical model to determine with high precision such penalty in disaggregated manner and with a conservative modeling of the filters. Within this context, we proposed a novel disaggregated approach to estimating the introduced effects in a real-world scenario related to the design of edge data centers, a critical aspect of fog computing development. Further analysis will be developed, considering more complex equalization techniques, finite taps equalizers, single-sided filtering and NLI, with an expansion of the measurement campaign and the aid of simulations.

Acknowledgment

This work has been partially funded by the EU - Next Generation EU under the Italian NRRP, Mission 4, Component 2, Investment 1.3, CUP E13C22001870001, partnership on "Telecommunications of the Future" (PE00000001 - program "RESTART") and by the Telecom Infraproject.

References

[1] Osanaiye, O. *et al.* "From Cloud to Fog Computing: A Review and a Conceptual Live VM Migration Framework", IEEE Access 2017.
[2] Puthal, D. *et al.* "Secure and Sustainable Load Balancing of Edge Data Centers in Fog Computing ", IEEE Communications Magazine 2018.
[3] Rizzelli, G. *et al.* "Experimental Demonstration of In-Field 400G Coherent Metro-Access Convergence", OFC 2024
[4] Kaneko, S. *et al.* "Photonic Gateway and Protocol-Independent End-to-End Optical-Connection Provisioning in All-Photonic Metro-Access Converged Network", IEEE 2023
[5] Virgillito, E. *et al.* , "Observation and Modeling of Filtering Penalties in Optical Switched Networks", ICTON 2024.
[6] Delezoide, C. *et al.* "Weighted Filter Penalty Prediction for QoT Estimation", OFC 2018.
[7] Mano, T. *et al.* "Modeling the Input Power Dependency of Transceiver BER-ONSR for QoT Estimation", OFC 2024.
[8] Agrawal, G.P. (2010) Fiber-Optic Communication Systems, John Wiley & Sons, New York.
[9] Proakis, J.G. and Salehi, M. (2008) Digital Communications. 5th Edition, McGraw-Hill, New York.
[10] Pulikkaseril, C. *et al.* "Spectral modeling of channel band shapes in wavelength selective switches", Optica Publishing Group 2011.
[11] Freude, W. *et al.* "Quality metrics for optical signals: Eye diagram, Q-factor, OSNR, EVM and BER", ICTON 2012.
[12] Carena, A. *et al.* "Modeling of the Impact of Nonlinear Propagation Effects in Uncompensated Optical Coherent Transmission Links", Journal of Lightwave Technology, 2012.